# Nanoscale

Accepted Manuscript


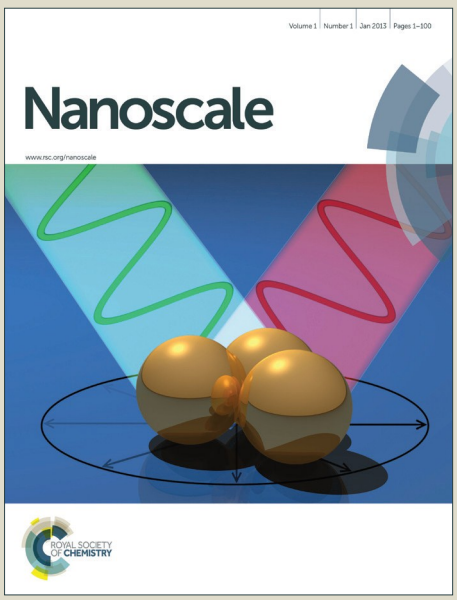





ROYAL SOCIETY OF CHEMISTRY

www.rsc.org/nanoscale

# SERS-active Sensor Based on Heterogeneous Gold Nanostar Core-Silver Nanoparticle Satellite Assemblies for Ultrasensitive Detection of AflatoxinB1

Aike Li[1*], Lijuan Tang[2], Dan Song[1], Shanshan Song[2], Wei Ma[2], Liguang Xu[2], Hua Kuang[2], Xiaoling Wu[2], Liqiang Liu[2], Xin Chen[3], Chuanlai Xu[2*]

A Surface-enhanced Raman scattering (SERS) sensor based on gold nanostar (Au NS) core-silver nanoparticle (Ag NP) satellites was fabricated for the first time to detect aflatoxinB1 (AFB1). We constructed the SERS sensor using AFB1 aptamer (DNA1)-modified Ag satellites and a complementary sequence (DNA2)-modified Au NS core. The Raman label (ATP) was modified onto the surface of Ag satellites. The SERS signal was enhanced when the satellite NP was attached to the Au core NS. The AFB1 aptamer on the surface of Ag satellites would bind to targets when AFB1 was present in the system, Ag satellites were then removed and the SERS signal decreased. This SERS sensor showed superior specificity for AFB1 and the detection linear range was from 1 to 1,000 pg/mL with the limit of detection (LOD) of 0.48 pg/mL. The excellent recovery experiment using peanut milk demonstrated that the sensor could be applied in food and environmental detection.

[1]*Cereals & Oils Nutrition Research Group, Academy of Science & Technology of State Administration of Grain, Beijing100037, PRC. E-mail: lak@chinagrain.org;*

[2]*State Key Lab of Food Science and Technology, School of Food Science and Technology, Jiangnan University, Wuxi, JiangSu, 214122, PRC. E-mail: xcl@jiangnan.edu.cn; Tel: 0510-85329076;*

[3]*Hubei Collaborative Innovation Center for Processing of Agricultural Products, Wuhan Polytechnic University, Wuhan,Hubei, 430023.*

## 1. Introduction

Aflatoxins (AF), which are secondary fungal metabolites, are a group of mycotoxins produced by *Aspergillus flavus* and *A. parasiticus*.[1] Aflatoxins are toxic and generally recognized as potent carcinogens, mutagens and teratogens.[2] The aflatoxins mainly include B1, B2, G1, and G2.[3] Of these, AFB1 has received considerable attention and is listed as a group I carcinogen by the International Agency for Research on Cancer (IARC) due to its abundance and high toxicity.[4] AFB1 is a widely-found residue in raw food materials, such as grains, corn, feedstuffs and peanuts. Exposure to a low level of AFB1 can cause immunosuppression and immunotoxicity, cancer, and even death. Thus, taking into account the risks of AFB1, regulatory limits for the level of this toxin have been established in many countries. In the United States and China, the current maximum allowed levels of AFB1 in foodstuffs is 20 ng/g.[5] Therefore, there is an urgent need to develop more robust methods for monitoring AFB1 levels in food to ensure food safety.

Conventional methods for AFB1 quantification in foodstuff samples have been developed and include liquid chromatography–tandem mass spectrometry (LC–MS/MS),[6] high-performance liquid chromatography–tandem mass spectrometry (HPLC–MS/MS)[7] and enzyme-linked immunosorbent assay (ELISA).[8] However, these methods are mainly based on instruments, are time-consuming, expensive, and require professional expertise. These drawbacks have limited their wide application. To solve these problems, various novel biosensors have also been developed.[9-12] For example, a colorimetric immunoassay, ultrasensitive aptasensor, photoelectrochemical immunosensor, and fluorescence sensor. Although these biosensor techniques, to some extent, have solved these problems, low sensitivity and stringent sample pretreatments need to be improved.

In recent years, Surface-enhanced Raman scattering (SERS) encoded noble metal nanomaterials have increased in popularity as important tools in biosensors.[13,14] However, the SERS signal of an encoded single nanomaterial was too weak for wide application in ultrasensitive detection. Although aggregations can largely improve the SERS signal, uncontrollable aggregation results in signal heterogeneity with low reproducibility of the SERS assay.[15] Therefore, controllable assemblies are critical in the fabrication of SERS-active sensors.[16] Many controllable assemblies have been fabricated, such as dimers,[17] trimers,[18] pyramids,[19] and chains.[20] Recently, core–satellite assemblies have gained increasing attention.[14,21] Our group has also fabricated a variety of core-satellite assemblies used in ultrasensitive detection. For example, Au-Ag NP core–satellite assemblies,[22] Au-UC NP core–satellite assemblies,[23] and Au NR-Au NP core–satellite assemblies.[24] However, to date, there are no reports on a SERS sensor using Au NS core–Ag NP satellite assemblies. Gold nanostars (Au NS) are an outstanding SERS substrate due to their anisotropic shape with the core and many tips.[25,26] The structure couples the plasmons focused on the multi-sharp tips which produce lots of ‘‘hotspots’’ that enhance the electromagnetic field around the particle.[27] Importantly, silver nanoparticles (Ag NPs) are also a good SERS candidate with significant SERS enhancement.[28] Therefore, in this study, we fabricated a new SERS sensor of Au NS core–Ag NP satellite assemblies using AFB1 aptamer (DNA1)-modified Ag satellites and a complementary sequence (DNA2)-modified Au NS core for AFB1 detection.[3]

## 2. Material and methods

### 2.1. Materials

Thiolated DNA aptamer was purchased from Shanghai Sangon Biological

Engineering Technology & Services Co. Ltd, China. The aptamer was purified by HPLC and suspended in deionized water from a Milli-Q device (18.2 MΩ, Millipore, Molsheim, France). Unless stated otherwise, all chemicals used in this study were purchased from Sigma–Aldrich.

The detailed sequences of the oligonucleotides are as follows:

AFB1 aptamer (DNA1):

HS-5'-GTTGGGCACGTGTTGTCTCTCTGTGTCTCGTGCCCTTCGCTAGGCCCAC -3'

Complementary sequence (DNA2):

HS-5'-CAGAGAGACAACACGTGCCCAAC -3'

## 2.2. Instrumentation

UV-Vis spectra were acquired using a UNICO 2100 PC UV-Vis spectrophotometer and processed with Origin Lab software. Transmission electron microscopy (TEM) images were obtained using a JEOL JEM-2100 operating at an acceleration voltage of 200 kV. Raman spectra were measured using a LabRam-HR800 Micro-Raman spectrometer with Lab-spec 5.0 software attached to a liquid cell. The slit and pinhole were set at 100 and 400 mm, respectively, in the confocal configuration, with a holographic grating (600 g/mm) and an air-cooled He-Ne laser giving 632.8 nm excitation with a power of ~ 8 mW. The spectrum resolution of Raman was ≤0.65 $cm^{-1}$ and the diameter of the laser spot was 7720.16 nm.

## 2.3. Synthesis of gold nanostars

Gold nanostars (Au NSs) were prepared from a seed-mediated growth method.[29] Initially, citrate solution (15 mL, 1%) was added into a boiling solution of HAuCl4 (100 mL, 1 mM) under vigorous stirring at 380°C. After reacting for 10 min, the seeds

were cooled to room temperature and then stored at 4°C. After the seed preparation, the Au NSs were fabricated.Silver nitrate ($AgNO_{3)}$ solution (200 μL, 3 mM), ascorbic acid solution (100 μL, 0.1 M), and 200 μL seeds were added to $HAuCl_4$ solution (20 mL, 0.25 mM) and quickly stirred for 1 min. The reaction was then terminated by centrifuging the colloidal solution at 3,000 rpm for 5 min. Finally, the precipitate was concentrated 10 times and then 0.01 M phosphate buffer (PBS) at a final concentration of 1 nM was added.

**2.4. Synthesis of silver nanoparticles**

Silver nanoparticles (Ag NPs) were prepared using a routine method with slight modifications. Initially, poly (N-vinyl-2-pyrrolidone) (PVP) (5 mL, 1%) and freshly prepared sodium borohydride ($NaBH_4$ ) (0.45 mL, 0.1 M) were mixed with 20 mL of distilled water. Next, $AgNO_3$ (5 mL, 10 mM) and PVP (5 mL, 1% by weight) were simultaneously injected into the mixture using a constant-flow pump at a rate of 30 mL/h under high-speed stirring. The reaction solution was kept at 80°C for 2 h to remove the unreacted $NaBH_4$ and then stored at 4°C.[30]

**2.5. Fabrication of DNA-modified Au NSs and Ag NPs**

Ag NPs were modified with AFB1 aptamer (DNA1) at a molar ratio of 4:1. Ag NPs were resuspended in 0.01 M PBS buffer at a final concentration of 10 nM by centrifugation. DNA1 (4 μL, 1 μM) was added to the Ag NPs solution (100 μL, 10 nM) under vigorous stirring. The Raman Label (4-ATP) solution was then added at a final concentration of 10 μM. After incubation at 37°C for 8 h, the particles were centrifuged at 13,000 rpm for 15 min and washed three times with PBS buffer (100 μL, 0.01 M). The deposit was collected and resuspended in 100 μL PBS buffer.

Au NSs were modified with AFB1 complementary (DNA2) at a molar ratio of 200:1. Briefly, DNA2 (2 μL, 10 μM) was added into the as-prepared Au NSs solution (100 μL, 1 nM). Then 5 M of NaCl solution was added at a final concentration of 500 mM under vigorous stirring. After reacting for 8 h, excess DNA was removed by centrifugation (three times) at 3,000 rpm for 5 min. The deposit was resuspended in 100 μL PBS buffer.

**2.6. Fabrication of the Au NS core–Ag NP satellite sensor**

Initially, 100 μL of prepared Ag NPs-DNA1 and 20 μL of prepared Au NSs-DNA2 were mixed under gentle shaking. Next, eight AFB1 standards were added at final concentrations of 0, 1, 2, 10, 50, 100, 500, and 1000 pg/mL, respectively. The solutions were then incubated at 37°C for 2 h. The Ag NPs were removed by centrifugation (three times) at 2,000 rpm for 3 min. Finally, TEM, UV−Vis and SERS spectroscopy were used to monitor this process.

**2.7. Analysis of specificity and selectivity**

Seven biotoxins (AFG1 (aflatoxin G1), AFG2 (aflatoxin G2), AFB2 (aflatoxin B2), M1 (aflatoxin M1), DON (deoxynivalenol), OTA (ochratoxin A), and FB1 (fumonisin B1)) were used to determine the specificity of the as-fabricated sensor. The concentrations of other analytes (100 ng/mL) were 100 times greater than that of AFB1 (1 ng/mL). All other detection procedures were identical to those used for AFB1.

**2.8. Recovery of AFB1 spiked in peanut milk samples**

The peanut milk was purchased from a local market and was confirmed to be negative

for AFB1 by the China Entry-Exit Inspection and Quarantine Bureau (CIQ) in Jiangsu. The peanut milk was centrifuged at 7,000 rpm for 10 min to remove fat from the supernatant. The milk was then diluted fivefold in PBS buffer, and both Ag NPs-DNA1 and Au NSs-DNA2 were added under vigorous stirring. The AFB1 standard sample at three concentrations (0.6, 3, and 6 pg/mL) were immediately added.

## 3. Results and discussion

### 3.1. Establishment of the heterogeneous core-satellites SERS-aptasensor for AFB1 detection

As illustrated in **Scheme 1**, firstly, DNA1-modified Ag NPs were mixed with DNA2-modified Au NSs. Following incubation for 2 h at 37°C, in the absence of AFB1, the Ag NP satellite assemblies with Au NS cores led to the formation of core-satellites architecture with an intense SERS signal. However, in the presence of AFB1 targets, the AFB1 aptamer (DNA1) prefers to switch its configuration to combine with the AFB1 target, which led to the release of complementary oligonucleotide (DNA2). Correspondingly, the core–satellites were disaggregated into dispersed nanoparticles with low SERS signals.

The Ag NPs, with a diameter of 8 nm, were synthesized by a routine method. The Au NSs, with a diameter of 45 nm, were prepared by a seed-mediated growth method. As shown in **Fig. 1**, the synthesized Ag NPs and Au NSs showed unique morphology and good dispersity. They also exhibited a localized surface plasmon resonance at 400 nm and 852 nm, respectively (**Fig. 2**). In order to fabricate the Au NS core–Ag NP satellite heterogeneous structure, the Ag NP satellites and Au NS cores were modified with DNA1 and DNA2 at a molar ratio of 4:1 and 200:1, respectively. According to

the fluorescence methods[31], the number of DNA1 and DNA2 coupled on Au NPs and Au NSs was calculated to be 1.1 ±0.4 and 23.6 ±0.9, respectively. Ag NP-DNA1 and Au NS-DNA2 were then mixed for 2 h. As shown in **Fig. 2**, the UV-Vis spectra of the core-satellites architecture compared with the spectra for Ag NPs and Au NSs showed no obvious change, which demonstrated that there were no large aggregations in this system. Furthermore, the assembled core satellites nanostructures were present in aqueous solution for 1 month in the absence of DNA cleaving enzymes. Therefore, the architecture can be applied as an aptasensor.

For AFB1 detection, eight AFB1 standards were added to the system containing Ag NP-DNA1-4-ATP and Au NS-DNA2 at final concentrations of 0, 1, 2, 10, 50, 100, 500, and 1,000 pg/mL, respectively. Following incubation for 2 h, the dissociated Ag NP-DNA1-4-ATP was removed by centrifugation (three times) at 2,000 rpm for 3 min. The representative TEM images of AFB1 at different concentrations are shown in **Fig. 3**. The number of Ag NPs surrounding Au NS in the presence of different concentration was statistically analyzed from more than 50 assemblies, respectively. As shown in **Fig. S1,** the number of Ag NP gradually was decreased with the concentration of target increased. In the sample without AFB1, the satellite Ag NPs completely surrounded the core Au NS, and had the highest assembly efficiency. However, there were no satellites around the core at the high concentration of AFB1 (1,000 pg/mL). The complexity and proportion of the assemblies in relation to the concentration of AFB1 were clearly seen. The UV-vis spectra at various concentrations of AFB1 are shown in **Fig. 4**. The absorbance spectra of these samples at 852 nm were not obviously different to each other. However, the absorbance spectra at 400 nm decreased when the concentration of AFB1 increased. This was because more Ag NPs could not assemble around the Au NSs when the concentration

of AFB1 increased, which led to dissociated Ag NPs being removed by centrifugation. This was further evidence that the AFB1 target can successfully combine with its aptamer to decrease the number of Ag NP satellites surrounding the core Au NSs. The change in UV-Vis spectra was not sensitive enough for quantitative determination. Therefore, the Raman spectrum was used to estimate the sensitivity of this sensor. The SERS intensity of 4-ATP significantly declined with increased concentration of AFB1, which corresponded to the decreased assembly of core satellites (**Fig. 5a**). Calibration curves were then plotted with the Raman signal at 1,136 $cm^{-1}$ as a logarithmic function of AFB1 concentration. A standard curve was obtained with an excellent correlation $R^2$ of 0.995 and a wide linear range from 1 to 1,000 pg/mL (**Fig. 5b**). The limit of detection was determined by three times the standard deviation of the blank solution and was calculated to be 0.48 pg/mL, which was lower than previously reported sensors.[2,3,5]

### 3.2. Specificity and selectivity of the sensor for AFB1 detection

To evaluate the selectivity and specificity of the as-fabricated sensor, seven biotoxins (G1, G2, AFB2, M1, DON, OTA, FB) were used. As illustrated in **Fig. 6**, the SERS signal was significantly decreased only when AFB1 was added. Although the concentrations of the other targets (100 ng/mL) were 100 times higher than AFB1 (1 ng/mL), no change in the SERS signal was observed. These results demonstrated that this method showed high selectivity for AFB1 detection.

### 3.3. Recovery of AFB1 spiked in peanut milk samples

To confirm the feasibility of this method, peanut milk samples were used as a substrate to perform AFB1 recovery experiments. The peanut milk samples were

purchased from a local market and were confirmed to be negative for AFB1 by Jiangsu Entry-Exit Inspection and Quarantine Bureau (CIQ) in. AFB1 standard solutions were added to the samples at a final concentration of 0.6, 3, and 6 pg/mL, and each spiked level was carried out for five parallel tests. As shown in **Table 1**, the recoveries of AFB1 were 88.33%–103.66%. And precision, expressed as the standard deviation, was assessed for five replicates with the same spiked samples (10.83%-18.33%). The results indicated that this assay would be useful for detect AFB1 residues in real samples.

## 4. Conclusion

In summary, we developed a simple and novel SERS-aptasensor for the detection of AFB1 based on heterogeneous Au NS core–Ag NP satellite nanostructures. This novel SERS sensor for the detection of AFB1 was fabricated for the first time. The sensor quantified the concentration of AFB1 with a limit of detection of 0.48 pg/mL and confirmed the feasibility and selectivity of this sensor. Therefore, we believe that this SERS sensor may have potential applications in the future.

## Acknowledgements

This work is financially supported by the Key Programs from MOST (2011BAD26B01-3, 2012YQ09019410, 2012BAD29B04), and grants from Natural Science Foundation of Jiangsu Province, MOF and MOE (BE2013613, BE2013611, 201310128, 201310135).

## References

1. Y. Lin, Q. Zhou, Y. Lin, D. Tang, G. Chen, D. Tang, *Biosens. Bioelectron.* 2015, 74, 680.

2. S. Srivastava, V. Kumar, M.A. Ali, P.R. Solanki, A. Srivastava, G. Sumana, P.S. Saxena, A.G. Joshi, B.D. Malhotra, *Nanoscale*. 2013, 5(7), 3043.
3. W.B. Shim, M.J. Kim, H. Mun, M.G. Kim, *Biosens. Bioelectron*. 2014, 62, 288.
4. X. Xu, X. Liu, Y. Li, Y. Ying, *Biosens. Bioelectron*. 2013, 47, 361.
5. W. Xu, Y. Xiong, W. Lai, Y. Xu, C. Li, M. Xie, *Biosens. Bioelectron*. 2014, 56, 144.
6. A. Bacaloni, C. Cavaliere, F. Cucci, P. Foglia, R. Samperi, A. Laganà, *J.Chromatogr. A*. 2008, 1179(2), 182.
7. W.S. Khayoon, B. Saad, T.P. Lee, B. Salleh, *Food. Chem.* 2012, 133(2), 489.
8. F.Y. Yu, A.V. Gribas, M.M. Vdovenko, I.Y. Sakharov, *Talanta.* 2013, 107, 25.
9. X. Guo, F. Wen, N. Zheng, Q. Luo, H. Wang, H. Wang, S. Li, J. Wang, *Biosens.Bioelectron.* 2014, 56, 340.
10. T. Li, J.Y. Byun, B.B. Kim, Y.B. Shin, M.G. Kim, *Biosens. Bioelectron.* 2013, 42, 403.
11. X. Wang, R. Niessner, D. Knopp, *Sensors*. 2014, 14(11), 21535.
12. S. Wu, N. Duan, C. Zhu, X. Ma, M. Wang, Z. Wang, *Biosens. Bioelectron*. 2011, 30(1), 35.
13. Y. Wang, B. Yan, L. Chen, *Chem. Rev*. 2013, 113(3), 1391.
14. Y. Zheng, T. Thai, P. Reineck, L. Qiu, Y. Guo, U. Bach, *Adv. Func. Mater.* 2013, 23(12), 1519.
15. S. Schlücker, *Angew. Chem. Int. Ed.* 2014, 53(19), 4756.
16. K. Liu, N. Zhao, E. Kumacheva, *Chem. Soci. Rev.* 2011, 40(2), 656.
17. K.D. Osberg, M. Rycenga, N. Harris, A.L. Schmucker, M.R. Langille, G.C. Schatz, C.A. Mirkin, *Nano. Lett*. 2012, 12(7), 3828.
18. S. Li, L. Xu, W. Ma, H. Kuang, L. Wang, C. Xu, *Small*. 2015, 11(28), 3435.
19. L. Xu, W. Yan, W. Ma, H. Kuang, X. Wu, L. Liu, Y. Zhao, L. Wang, C. Xu, *Adv. Mater.* 2015, 27(10), 1706.
20. W. Ma, H. Kuang, L. Xu, L. Ding, C. Xu, L. Wang, N.A. Kotov, *Nat. Commun.* 2013a, 4, 2689.
21. A. Shiohara, S.M. Novikov, D.M. Solís, J.M. Taboada, F. Obelleiro, L.M. Liz-Marzán, *The J. Phys. Chem. C*. 2015, 119(20), 10836.
22. X. Zhao, X. Wu, L. Xu, W. Ma, H. Kuang, L. Wang, C. Xu, *Biosens. Bioelectron*. 2015a, 66, 554.
23. X. Zhao, S. Li, L. Xu, W. Ma, X. Wu, H. Kuang, L. Wang, C. Xu, *Biosens. Bioelectron*. 2015b, 70, 372.
24. L. Xu, H. Kuang, C. Xu, W. Ma, L. Wang, N.A. Kotov, *J. Am. Chem. Soc*. 2012, 134(3), 1699.
25. S. Barbosa, A. Agrawal, L. Rodríguez-Lorenzo, I. Pastoriza-Santos, R.n.A. Alvarez-Puebla, A. Kornowski, H. Weller, L.M. Liz-Marzán, *Langmuir*. 2010, 26(18), 14943.
26. W. Ma, M. Sun, L. Xu, L. Wang, H. Kuang, C. Xu, *Chem. Commun*. 2013b, 49(44), 4989.
27. C. Hrelescu, T.K. Sau, A.L. Rogach, F. Jäckel, G. Laurent, L. Douillard, F. Charra, *Nano. Lett*.

2011, 11(2), 402.

28. J. Zhao, A.O. Pinchuk, J.M. McMahon, S. Li, L.K. Ausman, A.L. Atkinson, G.C. Schatz, *Acc. Chem. Res*. 2008, 41(12), 1710.
29. H. Yuan, C.G. Khoury, H. Hwang, C.M. Wilson, G.A. Grant, T. Vo-Dinh, *Nanotechnology*. 2012, 23(7), 075102.
30. X. Wu, L. Xu, L. Liu, W. Ma, H. Yin, H. Kuang, L. Wang, C. Xu, N.A. Kotov, *J.Am. Chem. Soc*. 2013, 135(49), 18629.
31. Hurst, S.J., Lytton-Jean, A.K.R., Mirkin, C.A., Anal. Chem. 2006, 78 (24), 8313–8318.

## Captions:

**Scheme 1** Scheme of AFB1 detection based on SERS method using Au NS core-Ag NP satellites assemblies.

**Fig. 1** TEM images of Ag NPs (a) and Au NSs (b).

**Fig. 2** The change of UV-Vis spectra of Ag NPs and Au NSs before and after assembly (A) and the changes of hydrodynamic size between Ag NPs and Ag NP-DNA1(B).

**Fig. 3** Representative TEM images of AuNS core-AgNP satellites assemblies in the presence of different concentrations of AFB1: (a) 0 pg/mL; (b) 1 pg/mL; (c)10 pg/mL; (d) 50 pg/mL; (e) 100 pg/mL; (f) 1000 pg/mL. Scale bar in the inset corresponds to 50 nm.

**Fig. 4** UV-Vis spectra of the probe in the presence of AFB1 ranging 0 from 1000 pg/mL.

**Fig. 5** (a) The SERS spectrum of 4-ATP with the different concentration of AFB1; (b) The standard curve based on 1136 $cm^{-1}$ frequency of 4-ATP.

**Fig. 6** Evaluation of the selectivity of SERS sensor at different target analytes. The concentration of AFB1 is 1 ng/mL, other analytes' are 100 ng/mL.

**Table 1** Recovery of AFB1 spiked in peanut milk samples

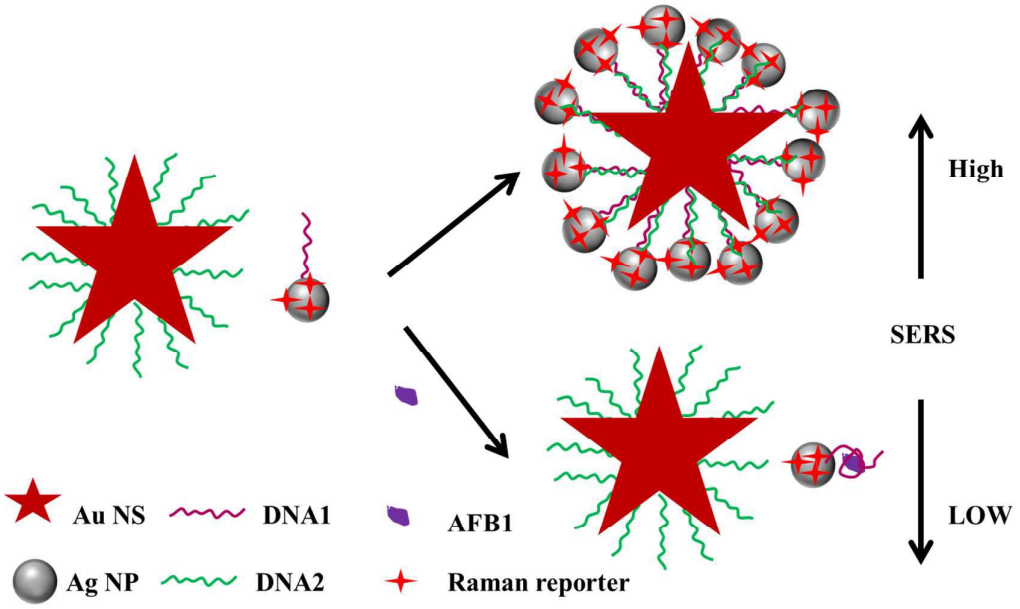


**Scheme 1** Scheme of AFB1 detection based on SERS method using Au NS core-Ag NP satellites assemblies.

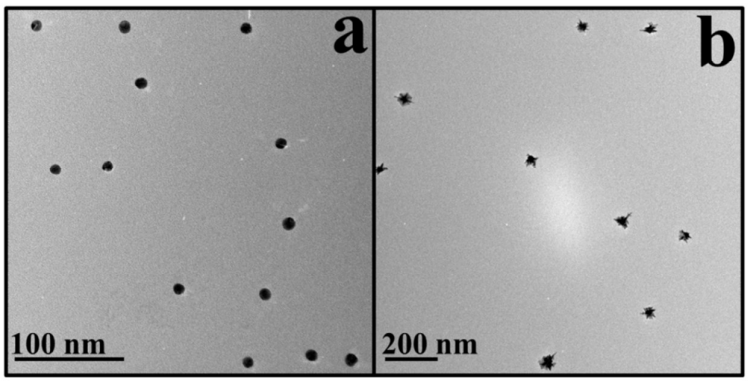


**Fig. 1** TEM images of Ag NPs (a) and Au NSs (b).

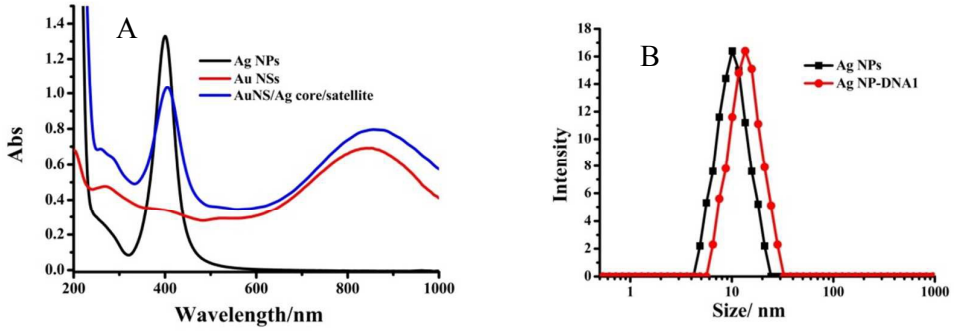


**Fig. 2** The change of UV-Vis spectra of Ag NPs and Au NSs before and after assembly (A) and the changes of hydrodynamic size between Ag NPs and Ag NP-DNA1(B).

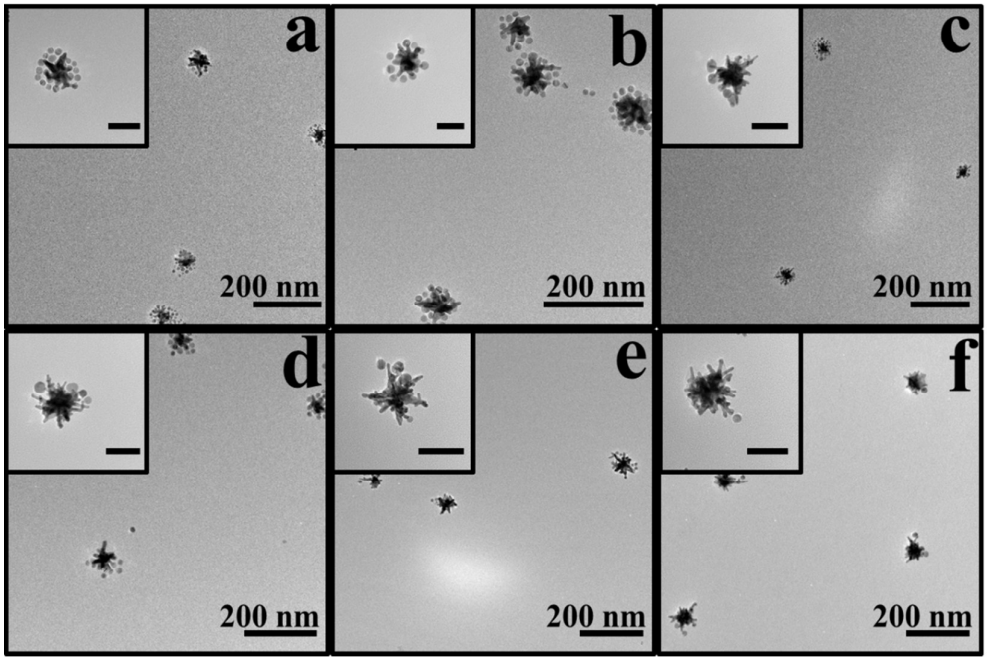


**Fig. 3** Representative TEM images of AuNS core-AgNP satellites assemblies in the presence of different concentrations of AFB1: (a) 0 pg/mL; (b) 1 pg/mL; (c)10 pg/mL; (d) 50 pg/mL; (e) 100 pg/mL; (f) 1000 pg/mL. Scale bar in the inset corresponds to 50 nm.

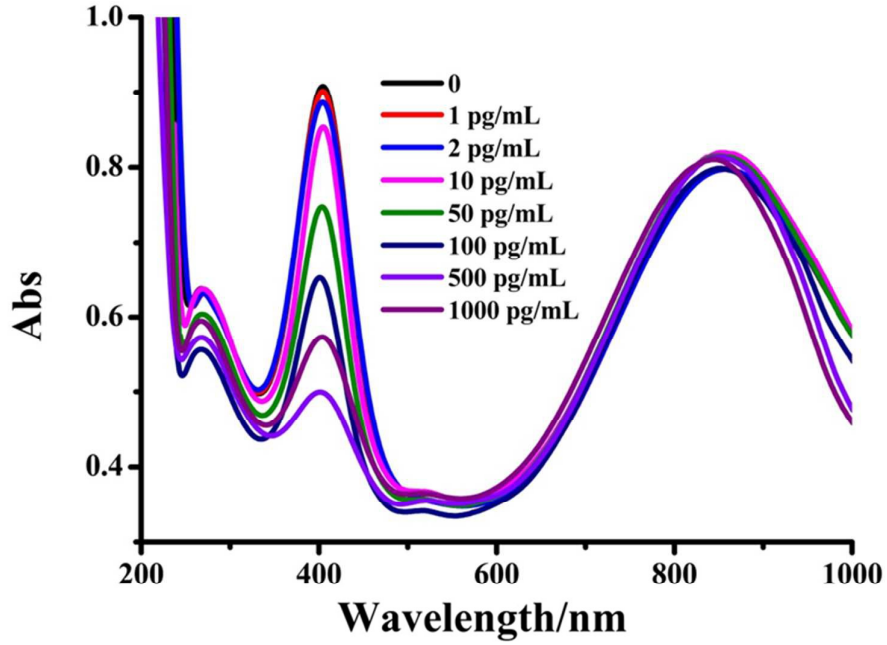


**Fig. 4** UV-Vis spectra of the probe in the presence of AFB1 ranging 0 from 1000 pg/mL.

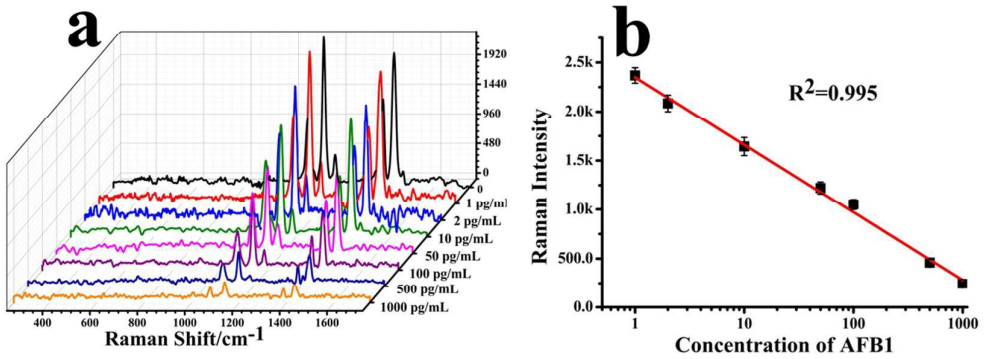


**Fig. 5** (a)The SERS spectrum of 4-ATP with the different concentration of AFB1; (b) The standard curve based on 1136 $cm^{-1}$ frequency of 4-ATP.

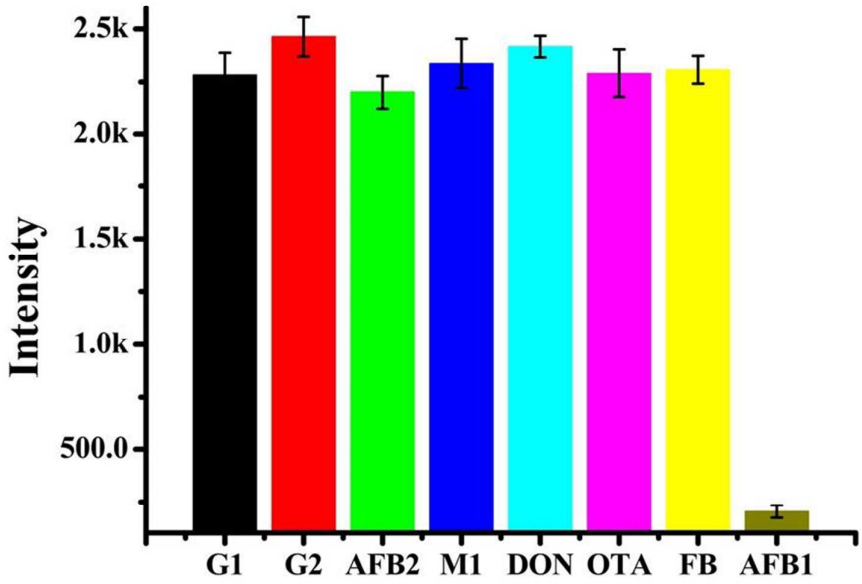


**Fig. 6** Evaluation of the selectivity of SERS sensor at different target analytes. The concentration of AFB1 is 1 ng/mL, other analytes' are 100 ng/mL.

**Table 1** Recovery of AFB1 spiked in peanut milk samples

| Sample | Spiked Concentration pg $mL^{-1}$) | Detected Concentration (Mean±SD, $ngmL^{-1}$, n = 5) | Recovery (%) (Mean±SD, n = 5) |
|---|---|---|---|
| Peanut milk | 0.6 | 0.53±0.11 | 88.33±18.33 |
| | 3 | 2.83±0.34 | 94.33±11.34 |
| | 6 | 6.22±0.65 | 103.66±10.83 |

# *Supporting information*

## Caption:

**Fig. S1** Representative TEM images of Au NS core-Ag NP satellites assemblies in the presence of different concentrations of AFB1 (Top), and statistical analysis of the number of Ag NPs surrounding Au NS in the presence of different concentrations of AFB1 (Bottom).

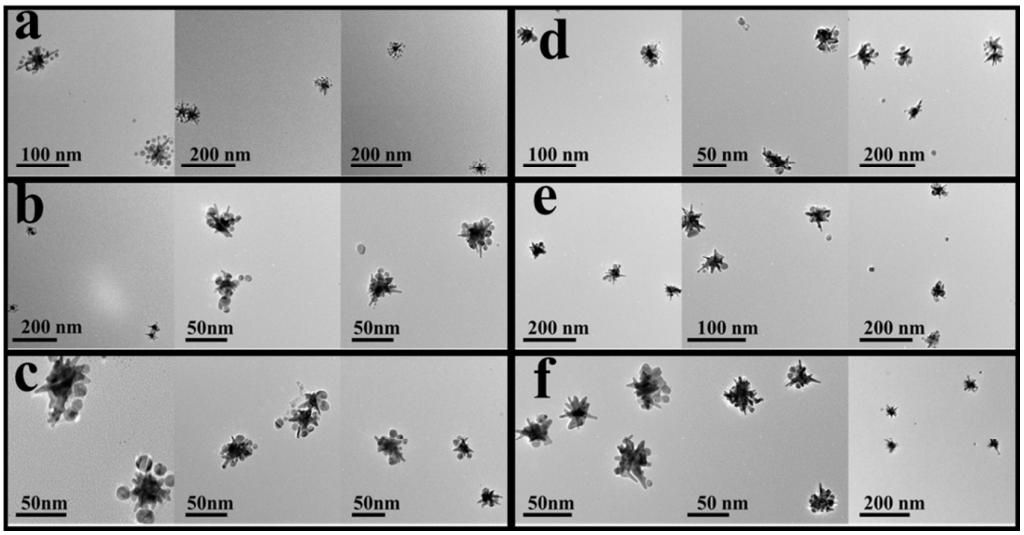


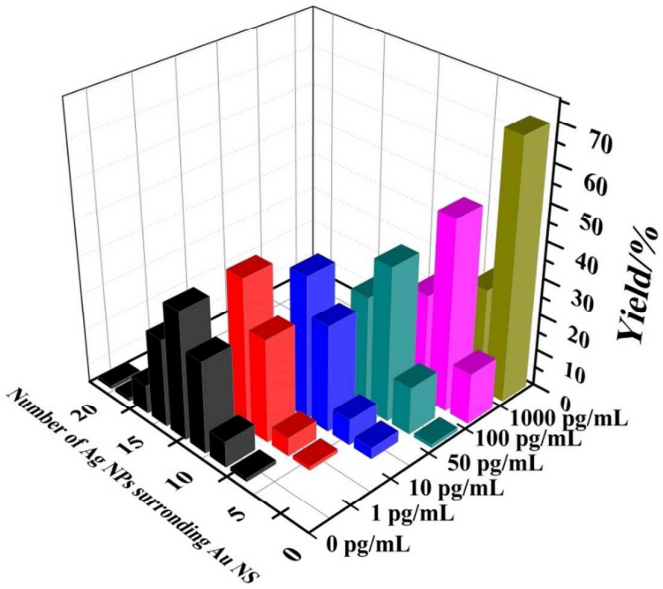


**Fig. S1** Representative TEM images of Au NS core-Ag NP satellites assemblies in the presence of different concentrations of AFB1: a) 0 pg/mL; b) 1 pg/mL; c) 10 pg/mL; d) 50 pg/mL; e) 100 pg/mL; f) 1000 pg/mL (Top), and statistical analysis of the number of Ag NPs surrounding Au NS in the presence of different concentrations of AFB1 (Bottom).